DOI: 10.1002/cphc.201000794

Ultrafast Vibrational Population Transfer Dynamics in 2-Acetylcyclopentanone Studied by 2D IR Spectroscopy

Sungnam Park*[a, b] and Minbiao Ji[c]

2-Acetylcyclopentanone (2-ACP), which is a β-dicarbonyl compound, undergoes *keto–enol* isomerization, and its *enol* tautomers are stabilized by a cyclic intramolecular hydrogen bond. 2-ACP (*keto* form) has symmetric and asymmetric vibrational modes of the two carbonyl groups at 1748 and 1715 cm^{-1}, respectively, which are well separated from the carbonyl modes of its *enol* tautomers in the FTIR spectrum. We have investigated 2-ACP dissolved in carbon tetrachloride by 2D IR spectroscopy and IR pump–probe spectroscopy. Vibrational population transfer dynamics between the two carbonyl modes were observed by 2D IR spectroscopy. To extract the population exchange dynamics (i.e., the down- and uphill population transfer rate constants), we used the normalized volumes of the cross-peaks with respect to the diagonal peaks at the same emission frequency and the survival and conditional probability functions. As expected, the downhill population transfer time constant (3.2 ps) was measured to be smaller than the uphill population transfer time constant (3.8 ps). In addition, the vibrational population relaxation dynamics of the two carbonyl modes were observed to be the same within the experimental error and were found to be much slower than vibrational population transfer between two carbonyl modes.

1. Introduction

Ultrafast two-dimensional infrared (2D IR) spectroscopy, which is a vibrational analogue of 2D NMR, offers a direct means to study dynamical processes occurring on the picosecond timescale in condensed phases by spreading spectral information over two frequency axes.[1–5] Experimentally obtained 2D IR spectra are displayed with the excitation and emission frequencies as a function of waiting time (T_w). As a result of many molecular processes, 2D IR spectra evolve as a function of T_w in terms of a change in peak shapes and an increase in the cross-peak amplitudes between corresponding diagonal peaks. For example, chemical exchange processes between two chemical species cause the cross-peaks to grow with increasing T_w.[6–10] Spectral diffusion dynamics lead to changes in peak shapes in T_w-dependent 2D IR spectra.[10–12] Due to the coherent population transfer between two coupled oscillators, their cross-peak amplitude oscillates at their frequency difference.[13] In addition, the incoherent population transfer between two coupled oscillators leads to gradual growth of their cross-peaks as a function of T_w.[14] By analyzing T_w-dependent 2D IR spectra, dynamical information on molecular systems of interest can be directly obtained.[3,15]

Both coherent and incoherent population transfer dynamics are of fundamental importance in understanding intramolecular vibrational redistribution, which has significant effects on the overall population relaxation dynamics of a vibrationally excited molecule. Coherent population transfer dynamics have been studied with metal carbonyl complexes. Tokmakoff and co-workers performed 2D dispersive vibrational echo (DVE) spectroscopy on the anharmonically coupled symmetric and antisymmetric carbonyl stretching modes of rhodium dicarbonyl complex [$Rh(CO)_2$(acac)] (acac = acetylacetonate) dissolved in chloroform.[16,17] They found that, due to vibrational coherence transfer, 2D DVE signals of [$Rh(CO)_2$(acac)] in chloroform were modulated with a period of 450 fs, which corresponded to the frequency separation (ca. 70 cm^{-1}) between its symmetric and antisymmetric carbonyl stretching vibrations, and the dephasing time of the coherence transfer between two vibrational modes was found to be 1.8 ps. More recently, Kubarych and co-workers studied [$Mn_2(CO)_{10}$] in cyclohexane solution[13] and observed that the amplitudes of the cross-peaks in its 2D IR spectra oscillated as a function of T_w with the frequency differences of the corresponding diagonal peaks, which revealed the signatures of the vibrational wave packet motions and coherence transfers among different vibrational modes.

Herein, we studied the (incoherent) population transfer dynamics in 2-acetylcyclopentanone (2-ACP) dissolved in CCl_4 by 2D IR spectroscopy and determined the population transfer time constants. As shown in Figure 1, 2-ACP is a β-dicarbonyl compound that undergoes *keto–enol* tautomerization in solution[18] and has two *enol* forms. The *enol* forms of 2-ACP are stabilized by a cyclic intramolecular hydrogen bond and are relatively stable in comparison to the *keto* form in CCl_4. The

[a] *Prof. Dr. S. Park*
Department of Chemistry
Korea University, Seoul 136-701 (Korea)
Fax: (+82) 2-3290-3121
E-mail: spark8@korea.ac.kr

[b] *Prof. Dr. S. Park*
Multidimensional Spectroscopy Laboratory
Korea Basic Science Institute, Seoul 136-713 (Korea)

[c] *M. Ji*
Department of Physics, Stanford University
Stanford, CA, 94305 (USA)

Supporting information for this article is available on the WWW under http://dx.doi.org/10.1002/cphc.201000794.

 © 2011 Wiley-VCH Verlag GmbH & Co. KGaA, Weinheim

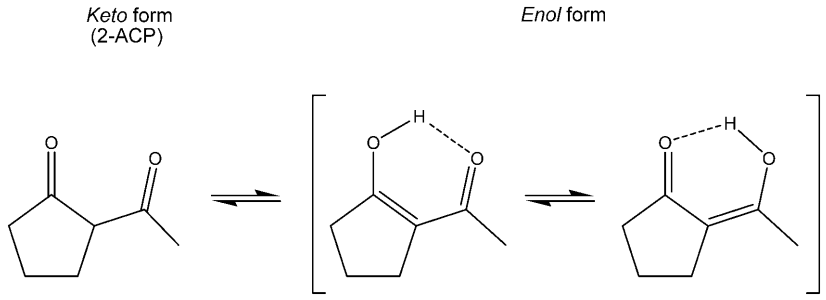

Figure 1. *Keto–enol* tautomerization of 2-ACP and intramolecular proton transfer in its *enol* forms.

two *enol* forms interconvert by intramolecular proton transfer, which is known to be much faster than *keto–enol* tautomerization. Kinetic studies on β-dicarbonyl compounds found the rate constants for *keto–enol* tautomerization in water to be on the order of 10^{-4}–10^{-3} s^{-1}.[19,20] Therefore, *keto–enol* tautomerization in 2-ACP occured on a much longer timescale than our experimental timescale.

The carbonyl stretching vibrations of 2-ACP and its *enol* forms were spectrally distinct and could be well separated in the FTIR spectrum (see Supporting Information). The carbonyl stretching vibrations of 2-ACP (*keto* form) were observed in a higher frequency region in the FTIR spectrum in comparison to its *enol* forms. Quantum chemical calculations were used to get detailed information on the carbonyl stretching vibrations. The two carbonyl groups in 2-ACP are weakly coupled and 2-ACP has spectrally distinct symmetric and asymmetric vibrational modes of the two carbonyl groups peaking at 1748 and 1715 cm^{-1}. The population transfer dynamics between two vibrational modes of 2-ACP were investigated by 2D IR spectroscopy. From the T_w-dependent 2D IR spectra, the downhill population transfer (1748→1715 cm^{-1}) time constant was determined to be 3.2 ps, and the uphill population transfer (1715→1748 cm^{-1}) time constant was 3.8 ps. The downhill population transfer was found to be faster. This suggests that the downhill population transfer is energetically more favorable and is more efficient than the uphill population transfer. The population relaxation dynamics of the two vibrational modes measured by polarization-controlled IR pump–probe experiments were found to be identical within the experimental error.

2. Results and Discussion

2.1. FTIR Spectroscopy

In solution, a β-diketone undergoes tautomerization and is in equilibrium with its *enol* form (*keto–enol* equilibrium). 2-ACP coexists with its *enol* forms in CCl_4. The *keto* and *enol* tautomers are spectrally distinct in the FTIR spectrum and can be selectively investigated. Detailed band analysis of FTIR spectrum of 2-ACP and its *enol* forms in CCl_4 is presented in the Supporting Information. The FTIR spectrum of 2-ACP (*keto* form) in CCl_4 is shown in Figure 2. For the remainder of the paper, the abbreviation 2-ACP refers to the *keto* form unless otherwise indicated. The two peaks shown in Figure 2 are well fitted by Lorentzian functions (see Supporting Information). The high-frequency, weak peak is centered at $\omega_A = 1748\ cm^{-1}$ with a bandwidth of $\Delta\omega_A = 15\ cm^{-1}$ (full width at half-maximum) while the low-frequency, intense peak is centered at $\omega_B = 1715\ cm^{-1}$ with $\Delta\omega_B = 11.7\ cm^{-1}$. The ratio of the extinction coefficients of the two peaks ($\varepsilon_B/\varepsilon_A = 1.96$) was determined by taking the ratio of their areas. For the purpose of simple interpretations, the high-frequency peak at 1748 cm^{-1} is assigned to the carbonyl stretching vibration of cyclopentanone, and the low-frequency peak at 1715 cm^{-1} to the carbonyl stretching vibration of the acetyl group.[21]

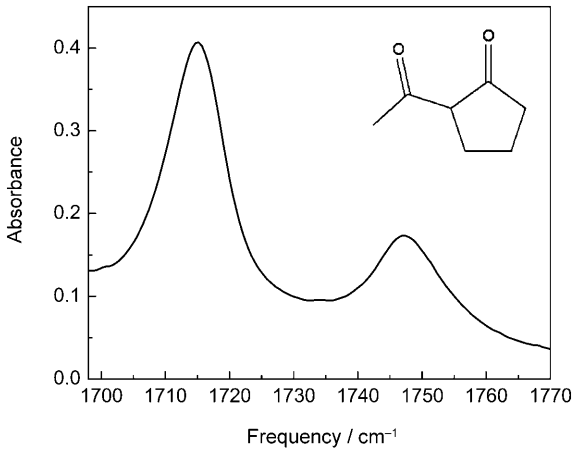

Figure 2. FTIR spectrum of 2-ACP in CCl_4. The high-frequency peak results from the symmetric stretching vibration of the two carbonyl groups, and the low-frequency peak from their asymmetric stretching vibration.

2.2. Quantum Chemical Calculations

To get more detailed information on these vibrational modes of 2-ACP, quantum chemical calculations were carried out by using the Gaussian 03 package.[22] Geometry optimization of 2-ACP and frequency calculations for its normal modes were performed by using the DFT method (B3LYP) with the 6-311+G(d,p) basis set in the gas phase. In the geometry-optimized structure of 2-ACP, the hydrogen atom of the acetyl group is very close to the carbonyl oxygen atom of cyclopentanone, and thus there appears to be an intramolecular interaction. The high-frequency peak was found to result from the symmetric stretching vibration of the two carbonyl groups, and the low frequency peak from their asymmetric vibration. However, for the high-frequency vibration, the carbonyl stretching vibration of the acetyl group has a larger amplitude, and for the low-frequency vibration the carbonyl stretching vibration of cyclopentanone has a larger amplitude. This indicates that

 © 2011 Wiley-VCH Verlag GmbH & Co. KGaA, Weinheim

the two carbonyl stretching modes are weakly coupled. In the calculated linear spectrum the high-frequency peak has lower intensity than the low-frequency peak, and this is qualitatively consistent with the measured FTIR spectrum. In addition, quantum chemical calculations were carried out to obtain the geometry-optimized structures and the frequencies of the normal modes for the two *enol* forms of 2-ACP, and the results were used to assign all the peaks in the measured FTIR spectrum of 2-ACP and its *enol* forms. (see Supporting Information for more details)

2.3. 2D IR Spectroscopy

Ultrafast 2D IR spectroscopy can monitor molecular dynamics on the picosecond timescale by vibrationally labeling the molecules with their initial frequencies (ω_τ) and then recording the final frequencies (ω_t) of the initially labeled molecules after an experimentally controlled waiting time (T_w).[6–8,23–27] 2D IR spectra $S(\omega_\tau,\omega_t,T_w)$ are displayed by correlating ω_τ and ω_t as a function of T_w. Figure 3 displays 2D IR spectra of 2-ACP in CCl_4 obtained at a series of T_w.

In Figure 3, the real parts of 2D IR spectra at different T_w are shown in the left column, and the corresponding absolute 2D IR spectra in the right column. In the real parts of 2D IR spectra, the red peaks along the diagonal ($\omega_\tau=\omega_t$) have positive amplitudes and result from the fundamental vibrational transition including the ground-state bleaching (GSB $v=0\rightarrow1$ transition) and stimulated emission (SE, $v=1\rightarrow0$ transition) contributions. The blue peaks below the diagonal are negative in amplitude and result from the excited-state absorption (ESA, $v=1\rightarrow2$ transition), and their frequencies are red-shifted from the diagonal along the ω_t axis by the vibrational anharmonicities. As mentioned above, the high-frequency diagonal peak (Peak A) at $\omega_\tau=\omega_t=1748\ cm^{-1}$ in Figure 3 results from the symmetric stretching vibration of the two carbonyl groups of 2-ACP, and its vibrational anharmonicity is about $21\ cm^{-1}$, while the low-frequency diagonal peak (Peak B) at $\omega_\tau=\omega_t=1715\ cm^{-1}$ comes from the asymmetric stretching vibration of the two carbonyl groups and its vibrational anharmonicity is about $12\ cm^{-1}$. In addition, the low-frequency peak is much more intense because it has a larger extinction coefficient.

It is clearly seen in Figure 3 that the cross-peaks grow gradually with increasing T_w. At $T_w=0.5$ ps, the peak at the upper left corner (Peak C) and that at the lower right corner (Peak D) are relatively weak. However, they become more intense as T_w increases. The cross-peaks result from vibrational population transfer between the two vibrational modes in 2-ACP. Cross-peak C results from the population transfer from Peak B (uphill transfer), and cross-peak D arises from population transfer from Peak A (downhill transfer). For the downhill population transfer, the excess vibrational energy is released to the solvent bath, while the energy required for the uphill population transfer is obtained from the solvent bath. Therefore, the downhill population transfer would be energetically more favorable. In the present case, the energy difference between Peak A and Peak B is much less than the thermal energy at room temperature. Therefore, the uphill and downhill population transfers would occur on similar timescales. The population transfer rate constants can be extracted by analyzing the cross-peak amplitudes as a function of T_w. A more quantitative analysis is presented in Section 2.5.

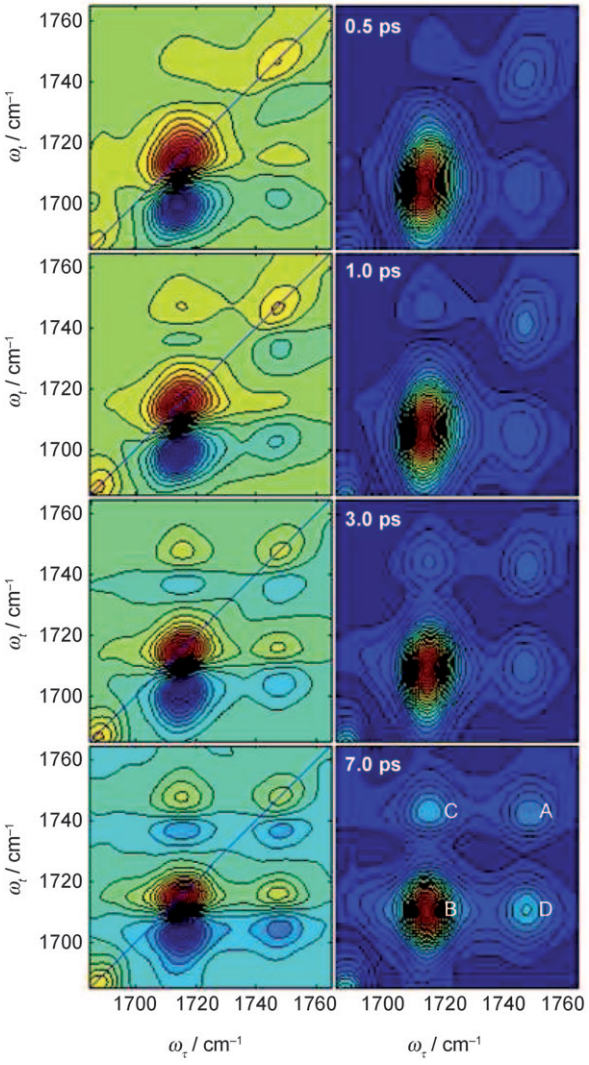

Figure 3. 2D IR spectra of 2-ACP measured at a series of T_w. Real parts of 2D IR spectra are in the left column and absolute 2D IR spectra are in the right column. It is clearly seen in the 2D IR spectrum at $T_w=7$ ps that Peaks A and B are diagonal peaks, while Peaks C and D are cross-peaks. The amplitudes of the cross-peaks increase gradually with increasing T_w.

2.4. IR Pump–Probe Spectroscopy

In IR pump–probe experiments, an IR pump pulse excites a molecular system to the first vibrational excited state ($v=1$), and subsequently the time evolution of the molecular system is measured by a time-delayed IR probe pulse. The IR pump–probe signal decays as a result of vibrational population relaxation and orientational relaxation. Polarization-controlled IR pump–probe experiments can be used to separately measure the vibrational population relaxation $P(t)$ and orientational relaxation dynamics $r(t)$. Figure 4 displays the population relaxation decays of the symmetric and asymmetric vibrations of the

 © 2011 Wiley-VCH Verlag GmbH & Co. KGaA, Weinheim

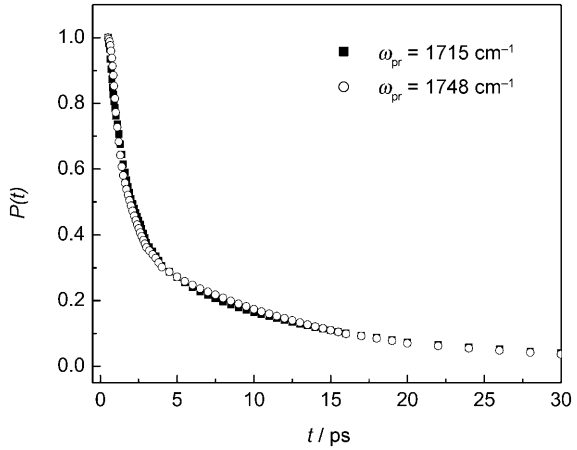

Figure 4. Population relaxation dynamics $P(t)$ of two vibrational modes measured at 1748 and 1715 cm^{-1} by polarization-controlled IR pump–probe experiments. Vibrational population decays of the two modes are found to be almost identical within the experimental error.

two carbonyl modes of 2-ACP measured at probe frequencies of 1715 and 1748 cm^{-1} (see Experimental Section for more details). The population decays $P(t)$ are fit by a bi-exponential function [Eq. (1)]:

$$P(t) = A\exp(-t/T_{1S}) + (1-A)\exp(-t/T_{1L}) \quad (1)$$

where T_{1S} and T_{1L} are the decay time constants with $T_{1S} < T_{1L}$. The fitting results are summarized in Table 1. The population decays of the two vibrational modes were found to be the same within experimental error. The orientational relaxation dynamics $r(t)$ measured at these two probe frequencies were also found to be identical, as expected.

Table 1. Results of biexponential fit to the population relaxation dynamics.

Probe frequency	A	T_{1S}	$1-A$	T_{1L}
1715 cm^{-1}	0.72±0.02	1.13±0.04	0.28±0.02	11.8±0.6
1748 cm^{-1}	0.74±0.02	0.96±0.04	0.26±0.02	11.9±0.6

2.5. Population Transfer Dynamics in 2D IR Spectra

Vibrational population transfer in a weakly coupled two-oscillator system can be described as in Figure 5. Two vibrational modes A (ω_A) and B (ω_B) are weakly coupled and their populations (energy) are transferred at the downhill (k_{AB}) and uphill (k_{BA}) population transfer rates, respectively. As a result of population transfer between two vibrational modes, the cross-peaks (Peaks C and D) between the two diagonal peaks (Peaks A and B) in the 2D IR spectra will grow gradually with increasing T_w, as shown in Figure 5.

The population transfer rates between A and B are related to the survival and conditional probability functions according to Equation (2):[14]

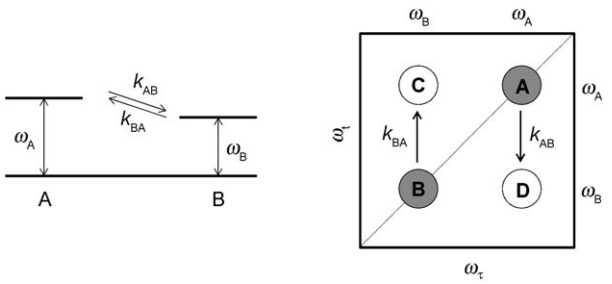

Figure 5. A weakly coupled two-oscillator system. A and B represent two oscillators with center frequencies of ω_A and ω_B, respectively. k_{AB} and k_{BA} are the downhill and uphill population transfer rate constants, respectively.

$$\begin{aligned} G_{AA}(t) &= \frac{k_{AB} + k_{BA}\exp(-k_{ex}t)}{k_{ex}} \\ G_{BB}(t) &= \frac{k_{BA} + k_{AB}\exp(-k_{ex}t)}{k_{ex}} \\ G_{AB}(t) &= \frac{k_{AB}[1-\exp(-k_{ex}t)]}{k_{ex}} \\ G_{BA}(t) &= \frac{k_{BA}[1-\exp(-k_{ex}t)]}{k_{ex}} \end{aligned} \quad (2)$$

where $k_{ex} = k_{AB} + k_{BA}$ is the population exchange rate constant, and $G_{AA}(t)$ and $G_{BB}(t)$ are the survival probability functions. For example, $G_{AA}(t)$ represents the probability of finding the system to be in state A at time t when the system was in the same state at time zero, and $G_{AB}(t)$, which is the conditional probability function, the probability of finding the system to be in state B at time t when the system was initially in state A at time zero.

In T_w-dependent 2D IR spectra, the vibrational population transfer rates were determined by analyzing how fast the cross-peak amplitudes grow with increasing T_w. Here, the absolute 2D IR spectra were used for quantitative analysis. Individual peaks in the absolute 2D IR spectra in Figure 3 were fit with 2D Gaussian functions and their volumes were numerically calculated. The amplitudes of individual peaks in the 2D IR spectra decay with increasing T_w as a result of population relaxation and orientational relaxation. In the 2D IR spectrum, the peaks at the same emission frequencies (ω_t) were assumed to have the same population relaxation and orientational relaxation rates. To remove the effect of population relaxation and orientational relaxation, the cross-peaks were normalized by dividing the volumes of the cross-peaks by those of the diagonal peaks at the same emission frequencies (ω_t) at each T_w. For example, at $T_w = 7$ ps, the volume of Peak C was divided by that of Peak A, and that of Peak D by that of Peak B.

The resultant normalized volumes of the cross-peaks are plotted against T_w in Figure 6. The change in the normalized volumes of the cross-peaks as a function of T_w time are directly associated with the population transfer rates. The intensities of the third-order signals are proportional to the fourth power of the transition dipole moments (i.e., the square of the extinction coefficients, $\varepsilon = \mu^2$) and the concentrations of chemical species. Therefore, the normalized volumes of the cross-peaks

 © 2011 Wiley-VCH Verlag GmbH & Co. KGaA, Weinheim

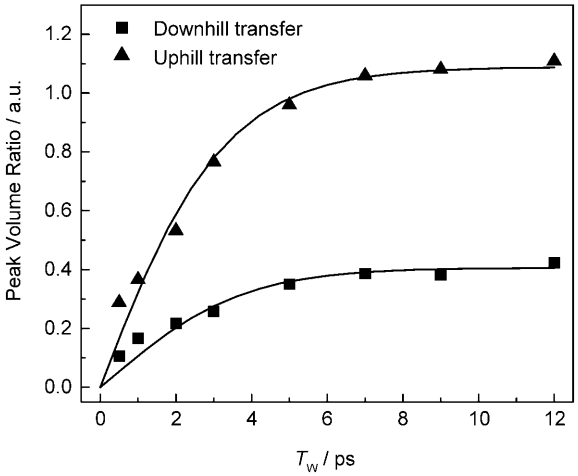

Figure 6. Normalized volumes of the cross-peaks (the volume ratios between the cross-peaks and the diagonal peaks) with respect to the diagonal peaks at the same emission frequency in the 2D IR spectra are plotted against T_w. Individual peak volumes are obtained by the 2D Gaussian fit. See text for more detail. The lines are fit by the model functions in Equation (3).

can be related to the survival and conditional probability functions in Equation (2) by Equation (3):[6–8,14,23–27]

$$\frac{V_D(T_w)}{V_B(T_w)} \propto \frac{\varepsilon_A G_{AB}(T_w)}{\varepsilon_B G_{BB}(T_w)}$$
$$\frac{V_C(T_w)}{V_A(T_w)} \propto \frac{\varepsilon_B G_{BA}(T_w)}{\varepsilon_A G_{AA}(T_w)} \quad (3)$$

where $V_\alpha(T_w)$ is the volume of Peak α in the 2D IR spectrum at a given T_w (see Figure 5), ε_A and ε_B are the extinction coefficients of A and B, respectively, and the ratio of the extinction coefficients is $\varepsilon_B/\varepsilon_A = 1.96$. To extract the downhill and uphill transfer rate constants (k_{AB} and k_{BA}) in Equation (2), the experimental results are simultaneously fit by the two equations in Equation (3) with a scaling factor. The lines in Figure 6 are the fit results. The downhill population transfer time constant is $\tau_{AB} = 1/k_{AB} = 3.2$ ps, and the uphill population transfer time constant was $\tau_{BA} = 1/k_{BA} = 3.8$ ps. The smaller downhill transfer time constant suggests that downhill transfer should be energetically more favorable and more efficient, as expected. The overall population exchange time constant is $\tau_{ex} = 1/k_{ex} = 1.7$ ps with $k_{ex} = k_{AB} + k_{BA}$.

The population transfer between two coupled vibrational modes occurs on the anharmonic potential surface when the two modes are simultaneously excited by the laser pulse. At very early times, the amplitude of the cross-peak between the two modes will oscillate due to the coherent population transfer. After the coherent population transfer decays out, population transfer takes place incoherently, and thus the cross-peak amplitude gradually increases relative to the diagonal peaks. The oscillatory frequency of the coherent population transfer is related to the frequency difference between the two anharmonically coupled oscillators, while the dephasing time gives information on how long the coherent population transfer between two modes takes places. In the case of 2-ACP, coherence transfer was not clearly observed in the 2D IR spectra and frequency-resolved IR pump–probe spectra. It is likely that the dephasing time of the coherence transfer in 2-ACP (a weakly coupled system) is much shorter than that of $[Rh(CO)_2(acac)]$ (1.8 ps) and $[Mn_2(CO)_{10}]$, such that the coherent population transfer decays out instantaneously upon IR excitation of the two carbonyl modes of 2-ACP and the incoherent population transfer is mainly observed in 2-ACP.

3. Conclusions

Herein, we have extensively studied the population dynamic of 2-acetylcyclopentanone (2-ACP) by ultrafast IR spectroscopy. 2-ACP is a β-dicarbonyl compound that undergoes *keto–enol* tautomerization in solution. In the FTIR spectrum of 2-ACP (*keto* form) and its *enol* forms in CCl_4, the carbonyl bands between 1600 and 1800 cm^{-1} were fully analyzed and assigned by using the results from quantum chemical calculations. Consequently, 2-ACP was spectrally distinguished from its *enol* forms. Vibrational population relaxation dynamics of the two vibrational modes of 2-ACP and vibrational population transfer dynamics between them were fully investigated by IR pump-probe and 2D IR experiments.

2D IR spectroscopy was carried out with 2-ACP in CCl_4, and population transfer dynamics between the vibrational modes of the two carbonyl groups were investigated. 2-ACP was modeled as a weakly coupled two-oscillator system. The symmetric stretching vibration of the two carbonyl groups in 2-ACP peaks at 1748 cm^{-1} with a smaller extinction coefficient, while the asymmetric stretching vibration of the two carbonyl groups peaks at 1715 cm^{-1}. Population transfer dynamics were directly monitored by measuring 2D IR spectra with increasing T_w. The population transfer rates were determined by analyzing the cross-peak amplitudes as a function of T_w. The normalized volumes of the cross-peaks were obtained from the 2D IR spectra and used to extract the downhill and uphill population transfer rates in combination with the conditional probability functions. The downhill population transfer time constant ($\tau_{AB} = 3.2$ ps) is smaller than the uphill population transfer time constant ($\tau_{BA} = 3.8$ ps). The vibrational population decays ($T_{1L} = 11.8$ ps) of two vibrational modes measured by polarization-controlled IR pump–probe experiments were found to be identical and occur on a longer timescale than the population exchange time ($\tau_{ex} = 1.7$ ps).

Vibrational population transfer dynamics are of critical importance in understanding intramolecular vibrational relaxation in polyatomic molecules. 2D IR spectroscopy can be performed with anharmonically coupled oscillator systems and utilized to extract direct information on population transfer dynamics by quantifying the cross-peak amplitudes in T_w-dependent 2D IR spectra. For strongly coupled oscillators, coherent population transfer is likely to be observed at early times, and the cross-peak amplitude in the T_w-dependent 2D IR spectra oscillates at the frequency difference between the two coupled oscillators with a decaying (damping) time constant. On the other hand, incoherent population transfer is mainly observed for weakly

 © 2011 Wiley-VCH Verlag GmbH & Co. KGaA, Weinheim

coupled oscillators, and the cross-peak amplitude gradually increases relative to the diagonal peaks associated with the two coupled oscillators.

Experimental Section

Sample Preparation: 2-Acetylcyclopentanone and carbon tetrachloride were purchased from Sigma-Aldrich and were used as received. 2-ACP (0.071 g) was directly dissolved in CCl_4 (5.0 g). The sample solution was housed in a cell consisting of two 3 mm-thick CaF_2 windows and a 100 μm-thick Teflon spacer and was used for all measurements. The FTIR spectrum of the sample solution was measured. The absorbances of the sample solution at 1715 and 1748 cm^{-1} were about 0.4 and about 0.17, respectively, after the solvent baseline was subtracted. 2D IR spectroscopy and polarization-controlled IR pump–probe experiments were performed with the sample solution at 22 °C.

Femtosecond Laser System: The laser system employed in the experiments was built on the basis of a design that has been described in detail elsewhere.[25] Briefly, 800 nm pulses were generated by a Ti:sapphire oscillator (KM Laser) and regenerative amplifier (Spitfire, Spectra-Physics) laser system at 1 kHz. The 800 nm pulses with 45 fs duration and about 0.8 mJ per pulse were used to pump an optical parametric amplifier (OPA, Spectra-Physics) to produce the signal and idler pulses at about 1.4 and about 1.9 μm, respectively, which were utilized to generate mid-IR pulses at 2050 cm^{-1} in a 0.5 mm-thick $AgGaS_2$ crystal by difference-frequency generation (DFG). The power spectrum of the mid-IR pulses had a Gaussian envelope with about 270 cm^{-1} bandwidth (full width at half-maximum). After generation, the mid-IR pulses propagated through an experimental setup that was purged with dry and CO_2-scrubbed air. The pulse chirp was measured by frequency-resolved optical gating (FROG) measurements in a transient grating geometry.[25] CaF_2 plates with different thicknesses were used to compensate for the linear dispersion introduced by other dielectric materials in the setup, particularly a Ge Brewster plate. This setup produced transform-limited mid-IR pulses with pulse duration of about 55 fs at the sample position.

2D IR Spectroscopy: The experimental details and principles of 2D IR spectroscopy have been described in detail elsewhere.[4,15,25,28] Three mid-IR pulses are focused with an off-axis parabolic mirror [focal length (f.l.) = 15 cm] onto the sample in a non-collinear geometry, and the beams are collimated after the sample with another off-axis parabolic mirror (f.l. = 15 cm). The spot size of the IR beams at the sample position is approximately 100 μm in diameter. The relative times of three incident pulses are controlled with motorized linear translational stages by a computer. The signal is emitted from the sample in a unique phase-matched direction. The emitted signal is overlapped with a local oscillator pulse for heterodyne detection. A grating in a spectrometer disperses the heterodyned signal onto the top stripe of a dual 32×2 element mercury cadmium telluride (MCT) array detector with high-speed data acquisition electronics (Infrared Associates and Infrared Systems Development Corp.). A portion of the IR beam that does not go through the sample is sent to the bottom stripe of the array and used as a reference beam. In 2D IR experiments, there are three experimental time variables. The delay between the first and second pulses corresponds to the evolution time (τ), the delay between the second and third pulses to the waiting time (T_w), and the delay between the third pulse and the emitted signal to the detection time (t). The 2D IR signal is measured by scanning τ at fixed T_w and frequency-resolving the heterodyned signal onto the array detector. Fourier transformations of τ and t are required to construct the 2D IR spectrum at a given T_w. The detection time t is Fourier transformed by the monochromator during the experiment to generate the ω_t axis, while τ is numerically Fourier transformed to produce the ω_τ axis after the τ-dependent interferogram is collected for each value of ω_t. Accordingly, 2D IR spectra are displayed with initial frequency ω_τ and final frequency ω_t at a fixed time T_w. Purely absorptive 2D IR spectra are measured with the dual-scan method, in which nonrephasing and rephasing 2D IR spectra are measured separately by two different input pulse sequences and added.[29]

Polarization-Controlled IR Pump–Probe Spectroscopy: The details of the IR pump–probe experiments have been described elsewhere.[12,26,30] Mid-IR pulses are split into pump and probe beams with relative intensity of 9:1 and are focused onto the sample. The probe beam is collimated after the sample and is dispersed through a spectrometer onto the MCT array detector. Wire-grid polarizers are placed in the pump and probe beam before the sample. The pump beam is horizontally polarized and the polarization of the probe beam is adjusted to be 45° with respect to the polarization of the pump beam. The analyzer wire-grid polarizer is inserted after the sample and is mounted on a computer-controlled motorized rotational stage. For individual scans, the analyzer polarizer is rotated by the computer to set the polarization of the signal to be parallel and perpendicular with respect to the polarization of the pump beam. The parallel, $S_{\parallel}(t)$, and perpendicular, $S_{\perp}(t)$, components of the pump–probe signals are alternatively measured with the polarization of the probe beam parallel and perpendicular to the pump beam, respectively. Then, the vibrational population relaxation is obtained by Equation (4):

$$P(t) = S_{\parallel}(t) + 2S_{\perp}(t) \tag{4}$$

and the orientational anisotropy is given by Equation (5):

$$r(t) = \frac{S_{\parallel}(t) - S_{\perp}(t)}{S_{\parallel}(t) + 2S_{\perp}(t)} = \frac{2}{5} C_{or}(t) \tag{5}$$

The orientational anisotropy $r(t)$ measures the orientational relaxation dynamics of the transition dipoles of the symmetric and asymmetric stretching vibrations as represented by the second-order Legendre polynomial of the transition dipole correlation function, $C_{or}(t) = \langle P_2[\boldsymbol{\mu}(t)\cdot\boldsymbol{\mu}(0)]\rangle$, while the population relaxation $P(t)$ measures the decays of the vibrationally excited molecules back to the ground state.

Acknowledgements

This research was financially supported by Basic Science Research Program through the National Research Foundation of Korea (NRF) funded by the Ministry of Education, Science and Technology (2010-0005020).

Keywords: 2D IR spectroscopy · coupled anharmonic oscillator · density functional calculations · population transfer dynamics · time-resolved spectroscopy

[1] M. Cho, *Chem. Rev.* **2008**, *108*, 1331 – 1418.
[2] J. Bredenbeck, J. Helbing, C. Kolano, P. Hamm, *ChemPhysChem* **2007**, *8*, 1747 – 1756.
[3] M. D. Fayer, *Annu. Rev. Phys. Chem.* **2009**, *60*, 21 – 38.

 © 2011 Wiley-VCH Verlag GmbH & Co. KGaA, Weinheim

[4] I. J. Finkelstein, J. Zheng, H. Ishikawa, S. Kim, K. Kwak, M. D. Fayer, *Phys. Chem. Chem. Phys.* **2007**, *9*, 1533 – 1549.
[5] N. T. Hunt, *Chem. Soc. Rev.* **2009**, *38*, 1837 – 1848.
[6] Y. S. Kim, R. M. Hochstrasser, *Proc. Natl. Acad. Sci. USA* **2005**, *102*, 11185 – 11190.
[7] S. Park, M. Odelius, K. J. Gaffney, *J. Phys. Chem. B* **2009**, *113*, 7825 – 7835.
[8] J. Zheng, K. Kwak, J. Asbury, X. Chen, I. Piletic, M. D. Fayer, *Science* **2005**, *309*, 1338 – 1343.
[9] S. Park, M. Ji, K. J. Gaffney, *J. Phys. Chem. B* **2010**, *114*, 6693 – 6702.
[10] I. J. Finkelstein, H. Ishikawa, S. Kim, A. M. Massari, M. D. Fayer, *Proc. Nat. Acad. Sci.* **2007**, *104*, 2637 – 2642.
[11] J. B. Asbury, T. Steinel, K. Kwak, S. A. Corcelli, C. P. Lawrence, J. L. Skinner, M. D. Fayer, *J. Chem. Phys.* **2004**, *121*, 12431 – 12446.
[12] S. Park, M. D. Fayer, *Proc. Natl. Acad. Sci. USA* **2007**, *104*, 16731 – 16738.
[13] M. J. Nee, C. R. Baiz, J. M. Anna, R. McCanne, K. J. Kubarych, *J. Chem. Phys.* **2008**, *129*, 084503.
[14] M. Cho, *Two-Dimensional Optical Spectroscopy*, CRC Press, Boca Raton, **2009**.
[15] J. Zheng, K. Kwak, M. D. Fayer, *Acc. Chem. Res.* **2007**, *40*, 75 – 83.
[16] N. Demirdöven, M. Khalil, O. Golonzka, A. Tokmakoff, *J. Phys. Chem. A* **2001**, *105*, 8025.
[17] N. Demirdöven, M. Khalil, A. Tokmakoff, *Phys. Rev. Lett.* **2002**, *89*, 237401.
[18] E. Iglesias, *New J. Chem.* **2002**, *26*, 1352 – 1359.
[19] E. Iglesias, *J. Org. Chem.* **2003**, *68*, 2680 – 2688.
[20] E. Iglesias, *New J. Chem.* **2005**, *29*, 625 – 632.
[21] D. L. Pavia, G. M. Lampman, G. S. Kriz, J. R. Vyvyan, Introduction to spectroscopy, Brooks/cole, Belmonte, **2009**.
[22] Gaussian 03 (Revision E.01), M. J. Frisch, G. W. Trucks, H. B. Schlegel, G. E. Scuseria, M. A. Robb, J. R. Cheeseman, J. A. Montgomery, Jr., T. Vreven, K. N. Kudin, J. C. Burant, J. M. Millam, S. S. Iyengar, J. Tomasi, V. Barone, B. Mennucci, M. Cossi, G. Scalmani, N. Rega, G. A. Petersson, H. Nakatsuji, M. Hada, M. Ehara, K. Toyota, R. Fukuda, J. Hasegawa, M. Ishida, T. Nakajima, Y. Honda, O. Kitao, H. Nakai, M. Klene, X. Li, J. E. Knox, H. P. Hratchian, J. B. Cross, V. Bakken, C. Adamo, J. Jaramillo, R. Gomperts, R. E. Stratmann, O. Yazyev, A. J. Austin, R. Cammi, C. Pomelli, J. W. Ochterski, P. Y. Ayala, K. Morokuma, G. A. Voth, P. Salvador, J. J. Dannenberg, V. G. Zakrzewski, S. Dapprich, A. D. Daniels, M. C. Strain, O. Farkas, D. K. Malick, A. D. Rabuck, K. Raghavachari, J. B. Foresman, J. V. Ortiz, Q. Cui, A. G. Baboul, S. Clifford, J. Cioslowski, B. B. Stefanov, G. Liu, A. Liashenko, P. Piskorz, I. Komaromi, R. L. Martin, D. J. Fox, T. Keith, M. A. Al-Laham, C. Y. Peng, A. Nanayakkara, M. Challacombe, P. M. W. Gill, B. Johnson, W. Chen, M. W. Wong, C. Gonzalez, J. A. Pople, Gaussian, Inc., Wallingford, **2004**.
[23] S. Woutersen, Y. Mu, G. Stock, P. Hamm, *Chem. Phys.* **2001**, *266*, 137 – 147.
[24] M. D. Fayer, D. E. Moilanen, D. Wong, D. E. Rosenfeld, E. E. Fenn, S. Park, *Acc. Chem. Res.* **2009**, *42*, 1210 – 1219.
[25] S. Park, K. Kwak, M. D. Fayer, *Laser Phys. Lett.* **2007**, *4*, 704 – 718.
[26] S. Park, D. E. Moilanen, M. D. Fayer, *J. Phys. Chem. B* **2008**, *112*, 5279 – 5290.
[27] J. F. Cahoon, K. R. Sawyer, J. P. Schlegel, C. B. Harris, *Science* **2008**, *319*, 1820 – 1823.
[28] M. Khalil, N. Demirdoven, A. Tokmakoff, *J. Phys. Chem. A* **2003**, *107*, 5258 – 5279.
[29] M. Khalil, N. Demirdoven, A. Tokmakoff, *Phys. Rev. Lett.* **2003**, *90*, 047401(047404).
[30] D. E. Moilanen, I. R. Piletic, M. D. Fayer, *J. Phys. Chem. C* **2007**, *111*, 8884 – 8891.

Received: September 27, 2010
Published online on February 7, 2011

 © 2011 Wiley-VCH Verlag GmbH & Co. KGaA, Weinheim